CHEMISTRY
A EUROPEAN JOURNAL

DOI: 10.1002/chem.200500355

Organolanthanide-Mediated Intermolecular Hydroamination of 1,3-Dienes: Mechanistic Insights from a Computational Exploration of Diverse Mechanistic Pathways for the Stereoselective Hydroamination of 1,3-Butadiene with a Primary Amine Supported by an *ansa*-Neodymocene-Based Catalyst

Sven Tobisch*[a]

Abstract: The complete catalytic reaction course for the organolanthanide-mediated intermolecular hydroamination of 1,3-butadiene and *n*-propylamine by an archetypical [$Me_2Si(\eta^5\text{-}Me_4C_5)_2NdCH(SiMe_3)_2$] precatalyst was critically scrutinized by employing a reliable gradient-corrected DFT method. A free-energy profile of the overall reaction is presented that is based on the thorough characterization of all crucial elementary steps for a tentative catalytic cycle. A computationally verified, revised mechanistic scenario is proposed which is consistent with the experimentally derived empirical rate law and accounts for crucial experimental observations. It involves kinetically mobile reactant association/dissociation equilibria and facile, reversible intermolecular diene insertion into the Nd–amido bond, linked to turnover-limiting protonolysis of the η^3-butenyl–Nd functionality. The computationally predicted effective kinetics ($\Delta H^{\neq}_{tot} = 11.3$ kcal mol^{-1}, $\Delta S^{\neq}_{tot} = -35.7$ e.u.) are in reasonably good agreement with experimental data for the thoroughly studied hydroamination of alkynes. The thermodynamic and kinetic factors that determine the almost complete regio- and stereoselectivity of the mechanistically diverse intermolecular 1,3-diene hydroamination have been unraveled. The present computational study complements experiments because it allows, first, a more detailed understanding and a consistent rationalization of the experimental results for the hydroamination of 1,3-dienes and primary amines and, second, enhances the insights into general mechanistic aspects of organolanthanide-mediated intermolecular hydroamination.

Keywords: hydroamination · density functional calculations · lanthanides · reaction mechanisms · regioselectivity

Introduction

Carbon–nitrogen and carbon–carbon bond-forming reactions are important fundamental transformations in synthetic chemistry. Catalytic hydroamination, that is, the addition of N–H bonds across unsaturated carbon–carbon functionalities, is a useful, direct, and atom-economical means of synthesizing nitrogen-containing compounds that have diverse applications as important bulk and fine chemicals or building blocks in organic chemistry.[1] A variety of complexes of early[2] and late[3] transition metals, as well as rare earth elements,[4] are known to assist the hydroamination reaction. Among them, lanthanides[5,6] exhibit a number of distinctive and useful characteristics for activation of carbon–carbon multiple bonds and amino groups. The unique properties of lanthanides include 1) the relatively large ionic radii, which give rise to high coordination numbers and possible coordinative unsaturation, 2) high electrophilicity and kinetic lability, 3) compatibility with a variety of nondissociable, immobile, yet tunable, ancillary ligation, and 4) a single stable oxidation state (Ln^{3+}). This opens a specific route for amine activation by transformation into the stronger nucleophilic amide **A** by deprotonation (Scheme 1). The amides of the strongly electropositive lanthanides can undergo nucleophilic addition to a C–C multiple bond to give a reactive intermediate **B** with pronounced carbanion activity. This intermediate is smoothly transformed into the alkylamine product (with regeneration of amide **A**) by concerted four-cen-

[a] Priv.-Doz. Dr. S. Tobisch
Institut für Anorganische Chemie
der Martin-Luther-Universität Halle-Wittenberg
Fachbereich Chemie, Kurt-Mothes-Strasse 2, 06210 Halle (Germany)
E-mail: tobisch@chemie.uni-halle.de

Supporting information for this article is available on the WWW under http:/www.chemeurj.org/ or from the author.

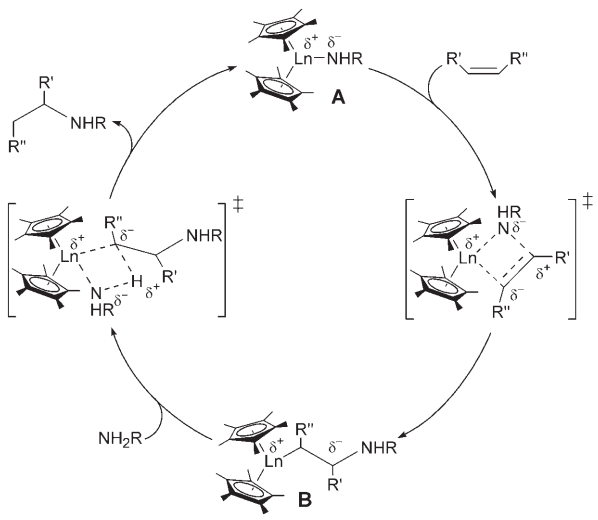

Scheme 1. Favorable route for amine activation through N–H deprotonation in the organolanthanide-supported hydroamination of unsaturated carbon–carbon functionalities. Apart from the shown intermolecular C–N bond formation, this process can also be accomplished in an intramolecular fashion.[7]

tered σ-bond metathesis, rather than by conventional oxidative addition/reductive elimination sequences, which are common in late transition metal chemistry.[1i]

Organolanthanides have been pioneered by Marks et al.[7] as highly efficient catalysts for the intramolecular cyclohydroamination of aminodienes[8] to regioselectively afford five-, six-, and seven-membered functionalized azacycles. The catalytic diversity of organolanthanide-mediated 1,3-diene hydroamination has been extended by Marks et al. to an intermolecular version,[9] which thus offers an efficient route to aliphatic aminoalkenes from readily available dienes and primary amines. The intermolecular hydroamination of 1,3-dienes by late transition-metal complexes has been advanced by Hartwig et al.[10] and Ozawa et. al.[11] Several computational studies dealing with transition-metal-assisted intermolecular hydroamination of a variety of substrates have been reported, whereby the work by Straub et al.[12a] and Senn et al.[12b] on early and late transition-metal catalysts, respectively, deserves particular attention.

Organolanthanide-mediated intermolecular hydroamination has been established for a variety of C–C multiply bonded systems,[9d] and is characterized by the following common features: 1) smooth precatalyst activation through protonolysis by amine substrate, 2) a large negative activation entropy ($\Delta S^{\neq}$), and 3) a reaction rate that is zeroth-order in [amine] and first-order in [hydrocarbon] and [catalyst].[7,9a,b] These observations suggest a similar turnover-limiting step for all intermolecular hydroamination processes, which Marks and Hong suggested to be bimolecular insertion of a C–C unsaturated bond into the Ln–N bond.[7] Although experimental studies led to the first detailed insights into intermolecular hydroamination, the nature of the turnover-limiting step and the origin of the high regio- and/or stereoselectivity, for instance, still require further elaboration. Thus, a thorough computational exploration can complement experiments by revealing intimate features, so that a symbiotic combination of computational and experimental approaches gives rise to the most detailed mechanistic picture.

Herein is presented, to the best of my knowledge, the first comprehensive computational study of the salient mechanistic features of the organolanthanide-supported intermolecular hydroamination of 1,3-dienes that comprises the complete sequence of crucial elementary steps. This study has a twofold aim: first, to unravel the general mechanistic principles of organolanthanide-assisted intermolecular hydroamination, with the intermolecular hydroamination of 1,3-dienes taken as an example, and second, to elucidate the principal catalytic issue of which factors govern the selectivity of the mechanistically highly diverse 1,3-diene hydroamination (see below). The following intriguing aspects are explored: 1) What are the crucial structural and energetic features of the individual elementary steps? 2) Which of the steps is likely to be assisted by excess diene and/or amine substrate? 3) Which species represents the resting state of the catalytic cycle? 4) Which step must be considered turnover-limiting? 5) Which factors determine the regioselectivity of the insertion and protonolysis steps? 6) What governs the almost complete stereospecificity?

The elucidation of these aspects allowed us to propose a computationally verified, revised mechanistic scenario that is consistent with the derived empirical rate law and rationalizes crucial experimental observations. The present study represents the first part of our systematic computational exploration of the fine mechanistic details and of the catalytic structure–reactivity relationships in the organolanthanide-assisted intermolecular hydroamination of a variety of unsaturated carbon–carbon functionalities.

Proposed Catalytic Reaction Course

Organolanthanide complexes of the general type $[Me_2SiCp'_2LnCH(TMS)_2]$ ($Cp' = \eta^5$-Me_4C_5; Ln = Nd, Sm, Lu; TMS = $SiMe_3$) have been reported to serve as effective precatalysts for the intermolecular hydroamination of 1,3-butadiene with primary amines.[9] Scheme 2 shows a general catalytic cycle for the organolanthanide-mediated intermolecular hydroamination of 1,3-butadiene with amine substrate **1** by $[Me_2SiCp'_2LnCH(TMS)_2]$ starting material **2**. Precatalyst **2** is activated through protonolysis by amine substrate **1** to afford amido–Ln complex **3** along with liberation of the hydrocarbyl ligand as $CH_2(TMS)_2$. Uptake of butadiene, which generates catalytically active diene–amido–Ln compound **4**, and subsequent insertion into the Ln–N bond gives rise to butenyl–Ln intermediates having a tethered amine functionality. With regard to the regio- and stereoselectivity, insertion can proceed along the alternative 1,2- and 1,4-routes, whereby butadiene can insert in either its s-*cis* or s-*trans* configuration, respectively. Insertion along the 1,4-route af-

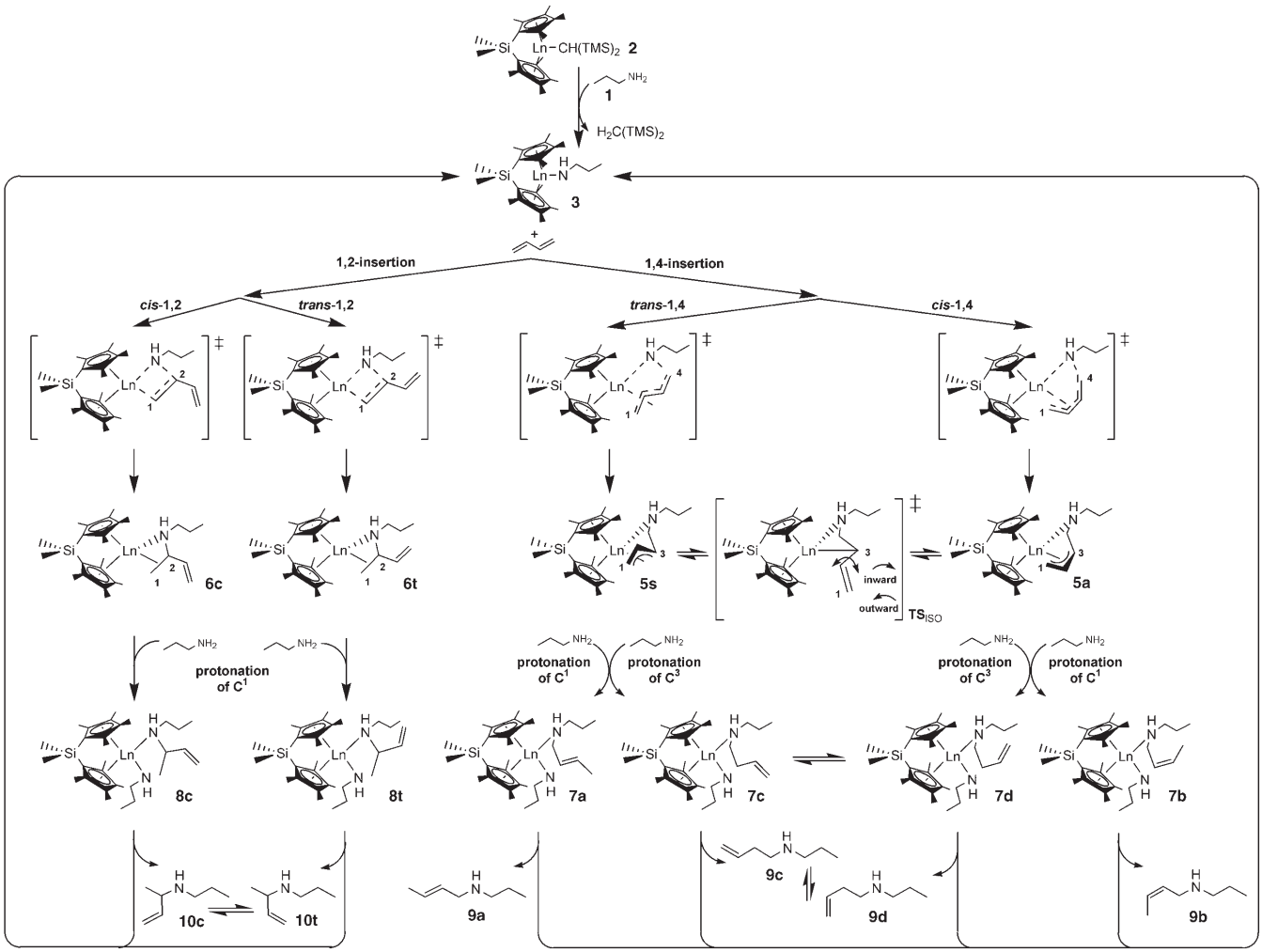

Scheme 2. General catalytic reaction course for the organolanthanide-mediated intermolecular hydroamination of 1,3-dienes and primary amines, based on experimental studies of Marks et al.[7,9] 1,3-Butadiene and *n*-propylamine (**1**), as well as $[Me_2SiCp'_2LnCH(TMS)_2]$ (**2**), were chosen as prototypical reactants and precatalyst, respectively. The diene–amido–Ln active catalyst complex **4** is omitted for the sake of clarity.

fords η^3-butenyl–Ln compound **5**,[6g,i,13,14] as stereoisomers **5s** (via the *trans*-1,4 pathway) and **5a** (via the *cis*-1,4 pathway), with *syn*- and *anti*-η^3-butenyl–Ln bonds. On the other hand, species **6t**, **6c** of the $\eta^1(C^2)$-butenyl–Ln regioisomer **6** are the products of the *trans*-1,2 and *cis*-1,2 insertion pathways, respectively. The two stereoisomers of **5** and **6**, respectively, are interconnected by allylic isomerization, as exemplified in Scheme 2 for **5s**⇌**5a**. The aminoalkene–amido–Ln complexes **7**, **8** are generated through ensuing protonolysis of the butenyl–Ln intermediates **5**, **6** by **1**, respectively, from which the aminoalkene products are readily liberated, thereby closing the catalytic cycle with regeneration of **3**. Protonolysis of **5** gives rise to linear aminoalkenes, while methyl-branched products are formed by protonation of **6**. Rotamers **10t**, **10c** of *N*-(1-methyl-2-propenyl)-*n*-propylamine are the products of the latter route that starts from **6t**, **6c**, respectively. Two different regioisomeric pathways are possible for protonolysis of **5s**, **5a**, in which the proton is transferred to either of the two reactive allylic sites. Protonation of the unsubstituted terminal C^1 carbon atom affords *N*-(*trans*-2-butenyl)-*n*-propylamine (**9a**) and *N*-(*cis*-2-butenyl)-*n*-propylamine (**9b**) isomers from **5s** and **5a**, respectively. The alternative proton transfer to the substituted C^3 carbon atom in **5s**, **5a** leads to rotamers **9c**, **9d** of *N*-(3-butenyl)-*n*-propylamine.

The intermolecular hydroamination of 1,3-butadiene and *n*-propylamine **1** by $[Me_2SiCp'_2NdCH(TMS)_2]$ (**2**) proceeds with almost complete stereospecificity, and **9a** is the aminoalkene that is almost exclusively formed.[9] Detailed kinetic studies on the intermolecular hydroamination of 1,3-dienes, however, have not been reported thus far. For the thoroughly investigated intermolecular hydroamination of alkynes with primary amines, experiment showed that the reaction rate is zeroth-order in [amine] and first-order in [alkyne] and [catalyst],[9a,b] as expressed in the empirical law [Eq. (1)], and associated with a large negative $\Delta S^{\neq}$ of

−25.9(9.7) e.u.[15] These findings can reasonably be adapted to the hydroamination of 1,3-dienes.

$$\text{velocity} = k[\text{amine}]^0[\text{alkyne}]^1[\text{Ln}]^1 \quad (1)$$

Computational Model and Method

Model: In this DFT study, the comprehensive computational exploration of the experimentally studied intermolecular hydroamination of 1,3-butadiene and *n*-propylamine **1** by $[Me_2Si(\eta^5\text{-}Me_4C_5)_2NdCH(SiMe_3)_2]$ precatalyst **2** is reported. Alternative regio- and stereoisomeric pathways for each of the crucial elementary steps of the tentative catalytic cycle shown in Scheme 2 have been scrutinized.

Method: All calculations were performed with the program package TURBOMOLE[16] using the BP86 functional,[17] which has already been applied successfully to the description of energetic and structural aspects of organolanthanide compounds[18] and has been furthermore demonstrated to allow the reliable determination of the energy profile for organolanthanide-assisted catalytic processes.[19] Further details together with a description of the employed computational methodology are given in the Supporting Information. All the drawings were prepared by employing the StrukEd program.[20]

Results and Discussion

The computational examination of 1,3-diene hydroamination is divided into two parts. It starts with the detailed step-by-step exploration of the various pathways conceivable for each of the elementary steps outlined in Scheme 2. This first part focuses on casting light on the crucial features of each of the individual steps. On the basis of the revealed detailed insights, in the second part, the condensed free-energy profile of the complete reaction is presented, and general mechanistic aspects of organolanthanide-promoted intermolecular hydroaminations are revealed. A further section is devoted to the implications regarding several issues of regio- and stereoselectivity of aminoalkene production.

Exploration of crucial elementary steps

Precatalyst activation: For the catalytic hydroamination to be initiated, precatalyst **2** requires activation through protonolysis by amine **1**, which converts it to amido-Ln complex **3** with liberation of the $CH_2(TMS)_2$ hydrocarbyl ligand. The key species participating along the favorable path for precatalyst activation are shown in Figure 1, while the energetics are collected in Table 1.

Protonolysis of **2** takes place with initial formation of amine substrate (AS) encounter complex **2**-AS and subsequent protonation of C^1 of the hydrocarbyl ligand. Amine complexation by **2** is an exothermic process ($\Delta H = -7.2$ kcal mol^{-1}, Table 1) that is, however, almost thermoneutral in terms of free energy ($\Delta G = 0.9$ kcal mol^{-1}), due to the entropic costs connected with bimolecular association. The transition state (TS) is encountered nearly halfway along the reaction path for proton transfer, as indicated by similar lengths of the vanishing N–H and emerging C–H

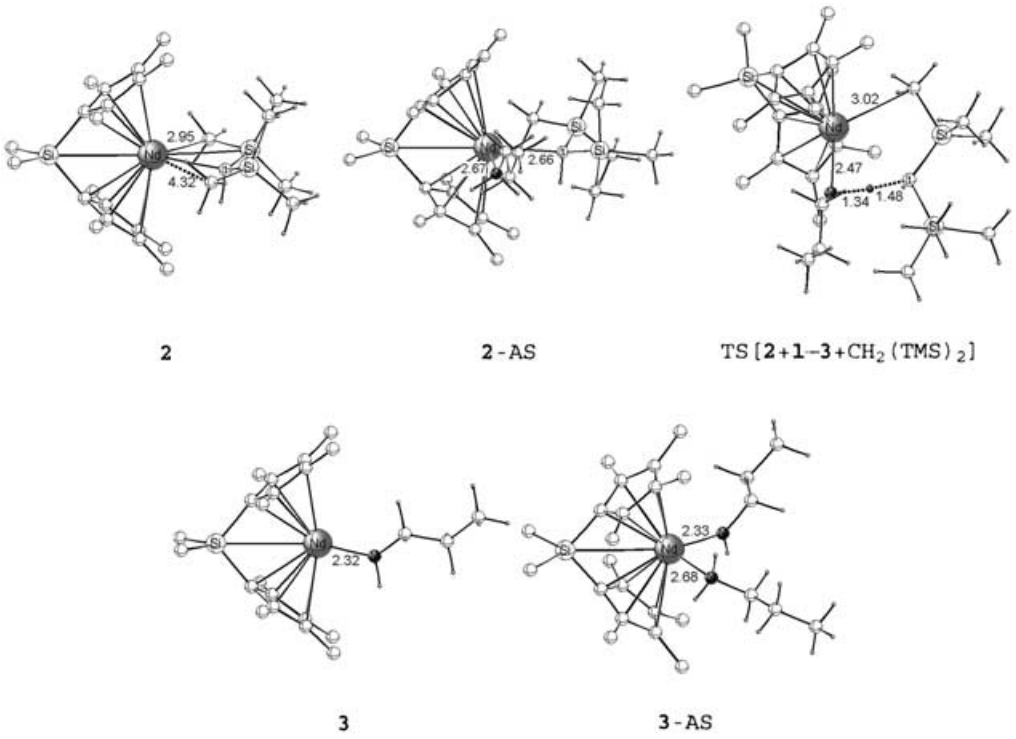

Figure 1. Selected geometric parameters [Å] of the optimized structures of key species for $\mathbf{1}+\mathbf{2}\rightarrow\mathbf{3}+CH_2(TMS)_2$ activation of precatalyst **2** through protonolysis by amine **1** (AS). The cutoff for drawing Nd–C bonds was arbitrarily set to 3.1 Å. The hydrogen atoms on the methyl groups of the catalyst backbone are omitted for the sake of clarity.

Table 1. Enthalpies and free energies of activation and reaction for protonolysis of precatalyst **2** by amine substrate **1**.[a,b]

Protonolysis pathway	Substrate encounter complex	TS	Products
1+**2**→ **3**+$CH_2(TMS)_2$	−7.2/*0.9* (**2**-AS)	3.2/*12.5* ($\Delta S^{\neq}=-31.2$ e.u.)[c]	−20.0/*−20.9* (**3**+$CH_2(TMS)_2$)
protonolysis pathway[e]		amine-substrate-assisted pathway[d] TS	
		9.6/*26.5* ($\Delta S^{\neq}=-56.6$ e.u.)[c]	

[a] Total barriers, reaction energies, and activation entropies are relative to {**1**+**2**}. [b] Activation enthalpies and free energies ($\Delta H^{\neq}/\Delta G^{\neq}$) and reaction enthalpies and free energies ($\Delta H/\Delta G$) are given in kilocalories per mole; values in italic type are the Gibbs free energies. [c] The activation entropy is given in entropic units (cal mol^{-1} K^{-1}). [d] The process assisted by an additive amine molecule was investigated with methylamine ($MeNH_2$, AS′) as substrate. Total barriers and activation entropies are relative to {**1**+**2**+$MeNH_2$}. [e] The additive substrate acts as a "proton shuttle" (see Figure S1, Supporting Information).

bonds in the located TS structure. Noteworthily, the TS is furthermore characterized by a significantly elongated Nd−C^1 bond, and thus by a loosely attached hydrocarbyl ligand (Figure 1). After overcoming a free-energy barrier of 12.5 kcal mol^{-1} (Table 1) the TS decays into **3** with smooth release of $CH_2(TMS)_2$, thereby activating the amine by transformation into the amido–Nd species. This process is driven by a strong thermodynamic force of −20.9 kcal mol^{-1} (ΔG), which implies that precatalyst activation proceeds in an almost quantitative fashion through initial **1**+**2**→**3**+$CH_2(TMS)_2$ protonolysis, which is kinetically feasible.

Inspection of the geometry of the key species reveals that **3** is potentially coordinatively unsaturated, so that it might have a tendency for complexation of excess substrate.[9c] Between butadiene and amine **1**, the latter, as the stronger donor, is found to be more competent in this regard (see Section 1.B) and gives rise to adduct **3**-AS, which is 6.6 kcal mol^{-1} lower in free energy than {**3**+**1**}. Accordingly, compound **3** predominantly occurs as amine adduct **3**-AS under actual reaction conditions.[9c]

The question whether an individual step benefits energetically from participation of excess reactants is of crucial importance for the interpretation of the experimental observations. For protonolysis, additive amine can be imagined reasonably, if at all, as being a supporting agent, since it, first, displays a higher tendency for complexation than butadiene and, second, is directly involved in the process. Additional amine molecules can assist protonolysis in different fashions, the most likely of which are, first, as a spectator by coordinative stabilization of the key species and, second, by directly involvement in the process as a mediator for proton transfer ("proton shuttle").[12b] The latter, direct amine assistance was explicitly probed computationally by locating the corresponding transition state (Figure S1, Supporting Information), in which methylamine was adopted as a chemically suitable and computationally affordable model amine. This transition state provides a clear insight into the role of the additional methylamine, which is seen to function as a mediating agent. Instead of a direct proton transfer as in TS[**2**+**1**–**3**+$CH_2(TMS)_2$] (Figure 1), the proton is transferred to C^1 from an external quarternary nitrogen center, which is generated by deprotonation of the terminal ammonium group of the Nd-coordinated substrate **1**. As revealed from Table 1, additional amine does not act to stabilize the transition state for protonolysis, either on the ΔH or on the ΔG surface, and this strongly indicates that excess reactants are unlikely to assist the first precatalyst activation step.

Intermolecular butadiene insertion into the Ln−N bond: After amine activation has proceeded smoothly with generation of amido–Nd complex **3**, butadiene uptake and ensuing insertion into the Nd−N bond are the next steps in the reaction course (Scheme 2). The complete energetics are collected in Table 2, and the key species for the 1,4-insertion are shown in Figure 2, while the structural data for the regioisomeric 1,2-path can be found in the Supporting Information (Figure S2). The first butadiene uptake affords the catalytically active diene–amido–Nd complex **4**. As previously analyzed,[18a] the interaction of a lanthanide with hydrocarbon π ligands is predominantly electrostatic in nature, and the resulting weak complexation of butadiene in **4** is characterized by rather long Nd−C distances and a diene moiety that is

Table 2. Enthalpies and free energies of activation and reaction for butadiene insertion into the Nd−N bond of **3** occurring along the alternative regioisomeric 1,2- and 1,4-pathways.[a,b]

Insertion pathway	π complex	TS	Product[c]
1,4-insertion			
cis-butadiene	3.3/*10.7* (**4**-1,4c)	5.2/*14.3* ($\Delta S^{\neq}=-30.5$ e.u.)[d]	−10.9/*−1.2* (**5a**)
trans-butadiene	−1.8/*5.5* (**4**-1,4t)	4.3/*13.4* ($\Delta S^{\neq}=-30.3$ e.u.)[d]	−10.5/*−0.7* (**5s**)
1,2-insertion			
cis-butadiene	0.8/*8.1* (**4**-1,2c)	12.6/*21.7* ($\Delta S^{\neq}=-30.5$ e.u.)[d]	5.3/*14.7* (**6c**)
trans-butadiene	−1.3/*6.3* (**4**-1,2t)	11.6/*20.7* ($\Delta S^{\neq}=-30.6$ e.u.)[d]	3.2/*12.5* (**6t**)
		amine-substrate-assisted process[e]	
1,4-insertion			
cis-butadiene		2.5/*19.1*	−10.4/*7.1* (**5a**-AS)
trans-butadiene		1.1/*18.0*	−13.7/*3.1* (**5s**-AS)
1,2-insertion			
cis-butadiene		9.9/*26.6*	1.8/*19.0* (**6c**-AS)
trans-butadiene		8.6/*25.2*	−1.6/*15.4* (**6t**-AS)

[a] Total barriers, reaction energies, and activation entropies are relative to {**3**+*trans*-C_4H_6}. [b] Activation enthalpies and free energies ($\Delta H^{\neq}/\Delta G^{\neq}$) and reaction enthalpies and free energies ($\Delta H/\Delta G$) are given in kilocalories per mole; values in italic type are the Gibbs free energies. [c] See Scheme 2 for description of the insertion products. [d] The activation entropy is given in entropic units (cal mol^{-1} K^{-1}). [e] The process assisted by an additional coordinating amine molecule was investigated for **1** as amine substrate (AS). Total barriers and reaction energies are relative to {**3**+*trans*-C_4H_6+**1**}.

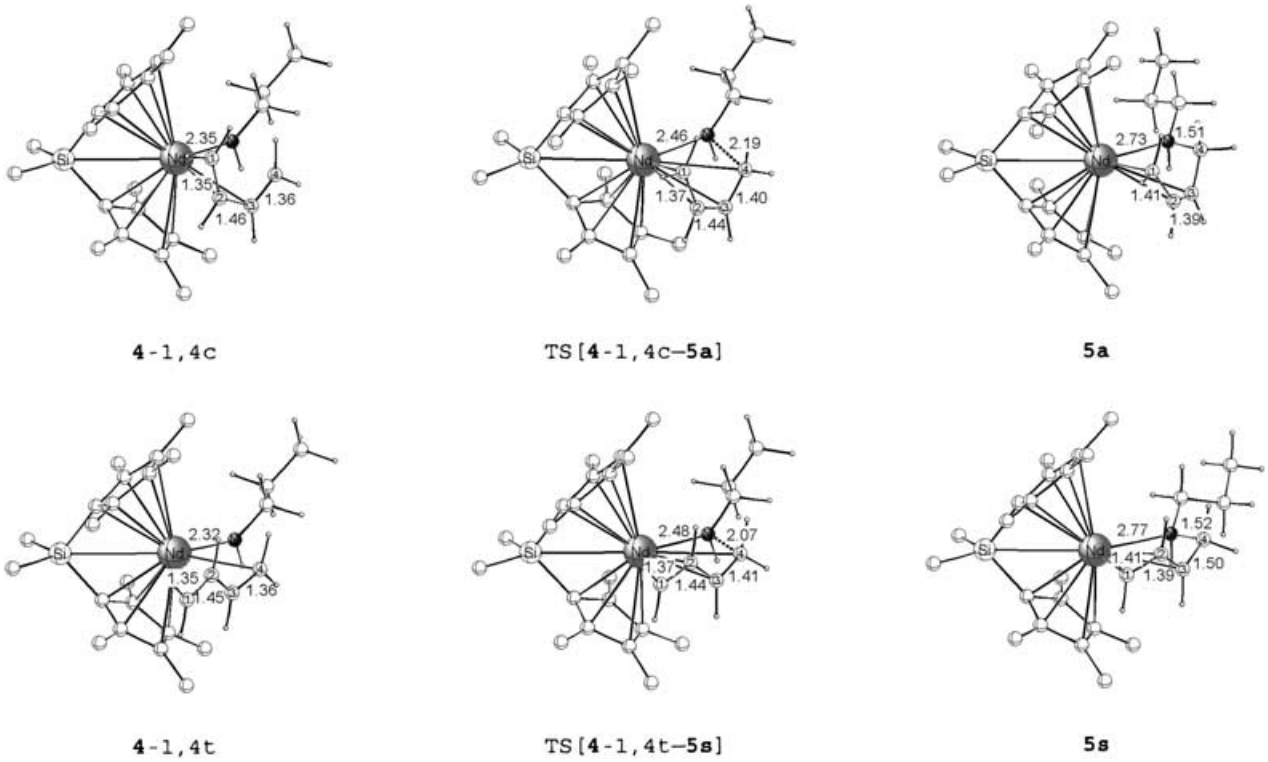

Figure 2. Selected geometric parameters [Å] of the optimized structures of key species for the stereoisomeric *cis*-1,4- (top) and *trans*-1,4-insertion (bottom) pathways. The cutoff for drawing Nd–C bonds was arbitrarily set to 3.1 Å. The hydrogen atoms on the methyl groups of the catalyst backbone are omitted for the sake of clarity.

only slightly distorted (Figures 2 and S2). The structural features are paralleled by the computed energetics (Table 2), which predict the uptake of *trans*- and *cis*-butadiene to be slightly exothermic and endothermic, respectively, on the ΔH surface relative to the separated {**3**+*trans*-C_4H_6} fragments. Since a chelating stabilization of *cis*-η^4-butadiene is not effective here, *cis*-butadiene complexation in "formal" monodentate (**4**–1,2c) and bidentate (**4**–1,4c) fashion is virtually equivalent energetically, whereby the latter is unfavorable due to some steric congestion around the Nd center. Noteworthily, the relative stability of the various forms of **4** (Table 2) reflects the stability of the s-*trans* and s-*cis* configurations of free butadiene.[21] Thus, the precursor species **4**–1,4c, **4**–1,4t, **4**–1,2c, **4**–1,2t for the various insertion pathways are likely to be present in different, but comparable populations. In terms of free energy, however, the bimolecular association suffers from an entropic penalty, and thus π-complex formation is thermodynamically unfavorable.

After butadiene uptake, insertion proceeds through a four-membered transition-state structure with a square-planar arrangement of the Nd–N and the inserting C=C functionality for both regioisomeric 1,4- and 1,2-insertion paths (Figures 2 and S2). On the 1,4-path C–N bond formation occurs at a distance of about 2.07–2.19 Å via TS[**4**-1,4t–**5s**] and TS[**4**-1,4c–**5a**], which are stabilized by partial π coordination of the already preformed allylic moiety. On the other hand, TS[**4**-1,2t–**6t**] and TS[**4**-1,2c–**6c**] for 1,2-insertion occur somewhat later at a distance of about 1.96–1.98 Å of the newly formed C–N bond and constitute the insertion of η^2-vinylethylene into the Nd–N bond. The decay of the transition states gives rise to **5s**, **5a** along the 1,4-path, which have a *syn*- and an *anti*-η^3-butenyl group, respectively, together with the coordinated N-donor center of the tethered amine moiety. The $\eta^1(C^2)$-butenyl-Nd compounds **6t**, **6c** with an η^1-coordinated amino group are the products of the 1,2-path (Scheme 2, Figures 2 and S2).

The stabilizing effect of the η^3-π mode of butenyl–Nd coordination, when compared to the η^1-σ mode, is clearly seen from the relative stabilities of the TS and of the insertion products that are associated with the various pathways. The 1,4-path is distinctly favored, both kinetically ($\Delta\Delta G^{\neq} > 7$ kcal mol^{-1}) and thermodynamically ($\Delta\Delta G > 13$ kcal mol^{-1}), relative to 1,2-insertion. This leads to the conclusion that generation of **6t**, **6c** by 1,2-insertion is entirely precluded energetically, and **5s**, **5a** are the exclusive products of the insertion step. Along the dominant 1,4-path, almost identical energy profiles are predicted for the *trans*-1,4 and *cis*-1,4 pathways, that is, both are equally likely to be traversed.[22] Coordination of the amine-N atom to Nd, as realized in the favorable isomers of **5s**, **5a** (Figure 2), affects significantly the stability of these species. Isomers with a disrupted Nd–N interaction are strongly disfavored energetically (>5–9 kcal mol^{-1} higher in free energy).

Before firm conclusions about the regio- and stereoselective outcome of the insertion can be drawn, it must be elucidated whether excess substrates[9c] can act competently to

support the process. This has been probed computationally for both **1** and butadiene. As already indicated by the weak butadiene association in **4**, additional butadiene molecules do not exhibit any tendency to stabilize either of the key species by complexation. Despite several efforts, all attempts to localize such species failed, and this provides strong indications that excess butadiene does not facilitate the insertion energetically. With regard to amine as a possible assisting agent, the various insertion pathways were explored with explicit participation of *n*-propylamine (**1**) (Figure S3, Supporting Information). The complete energetics are included in Table 2. As exemplified for the dominant 1,4-path, amine complexation in the TS and in **5** comes at the expense of the butenyl–Nd coordination, which for the TS switches from an η^3-π toward an η^1-σ mode. Despite several attempts, amine adducts of precursor **4** could not be located. Thus, excess amine is not likely to participate in the early stages, but is possibly involved when the process approaches the vicinity of the transition state. As far as the ΔH surface is concerned, the kinetics and reaction energy benefit to only a small extent from amine association, as TS-[**4**-1,4–**5**]-AS and **5**-AS are stabilized at most by 3.2 kcal mol^{-1} relative to {TS[**4**-1,4–**5**]+**1**} and {**5**+**1**}, respectively. The magnitude of the enthalpic profit is certainly not large enough to compensate for the entropic disfavor connected with amine association, so that a free-energy profile arises for the amine-assisted process that is more difficult than for **3**+C_4H_6→**5**. Accordingly, it must be concluded that neither excess butadiene nor amine substrate is likely to assist the insertion step.

Overall, butadiene insertion is predicted to be almost thermoneutral in terms of free energy, is thus likely to occur in a reversible fashion, and must overcome an activation barrier of 13.4–14.3 kcal mol^{-1} ($\Delta G^{\neq}$). C–N bond formation occurs with complete regioselectivity along the 1,4-path, and the stereoisomeric *trans*-1,4 and *cis*-1,4 pathways are equally feasible, both kinetically and thermodynamically. Thus, **5s** and **5a** are formed as intermediates of the catalytic process and should be present in similar concentrations. As anticipated, a large negative activation entropy ($\Delta S^{\neq} = -(30.3–30.5)$ e.u., Table 2) is linked to this bimolecular step.

Isomerization of the allylic group of the 1,4-insertion product: Although **5s** and **5a** are generated through alternative insertion pathways and are likely to have similar populations, it is of mechanistic interest whether the two isomers are readily interconvertible by allylic isomerization. This process is found to preferably proceed through initial η^3-π→η^1-σ switching of the butenyl–Nd coordination mode and subsequent internal rotation of the vinyl group around the formal C^2–C^3 single bond via TS_{ISO}[**5**]. This is in agreement with evidence provided by both experimental[23,24] and computational[25] studies. The key species involved along the preferable pathway for **5s**⇌**5a** interconversion are shown in Figure 3, and the energy profile is collected in Table 3.

Table 3. Enthalpies and free energies of activation and reaction for allylic isomerization occurring in compound **5**.[a,b]

Insertion pathway	**5s**[c]	TS_{ISO}	**5a**[c]
1,4-insertion	0.0/*0.0*	18.4/*18.2* ($\Delta S^{\neq}$ = 0.6 e.u.)[d]	−0.4/*−0.5*
		amine-substrate-assisted process[e]	
1,4-insertion	−3.2/*3.8* (**5s**-AS)	11.1/*19.2* ($\Delta S^{\neq}$ = −27.0 e.u.)[d]	0.1/*7.9* (**5a**-AS)

[a] Total barriers, reaction energies, and activation entropies are relative to the *syn*-η^3-allyl-Ln isomer **5s**. [b] Activation enthalpies and free energies ($\Delta H^{\neq}/\Delta G^{\neq}$) and reaction enthalpies and free energies ($\Delta H/\Delta G$) are given in kilocalories per mole; values in italic type are the Gibbs free energies. [c] See the text (or Scheme 2) for description of the isomers of **5**. [d] The activation entropy is given in entropic units (cal mol^{-1} K^{-1}) [e] The process assisted by an additional coordinating amine molecule was investigated for **1** as the amine substrate (AS). Total barriers, reaction energies and activation entropies are relative to {**5s**+**1**}.

The η^3-π→$\eta^1(C^3)$-σ butenyl–Nd rearrangement lowers the coordination number around the lanthanide center. As seen from Figure 3, this is partially compensated for in TS_{ISO}[**5**] by an amplified interaction between Nd and the lone pair of the amino nitrogen atom. Nevertheless, thermoneutral **5s**⇌**5a** isomerization is predicted to be kinetically difficult, associated with a significant free-energy barrier of 18.2 kcal mol^{-1} (Table 3), which, however, is of the same magnitude

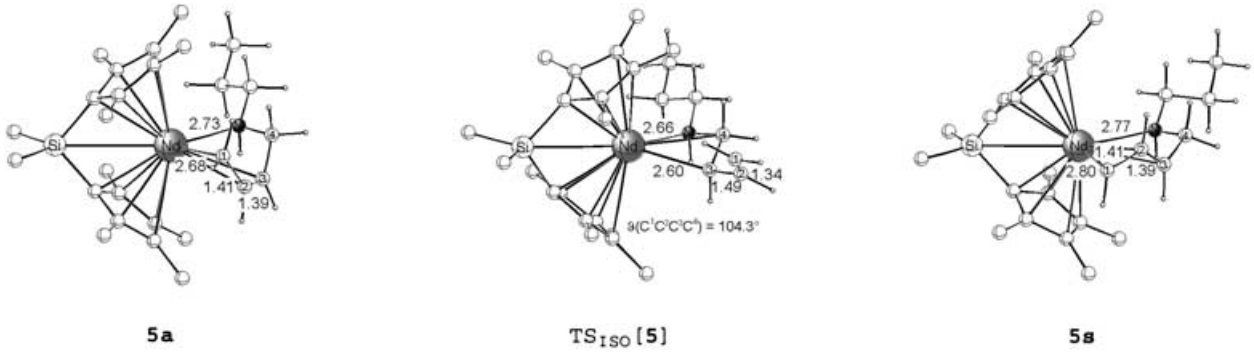

Figure 3. Selected geometric parameters [Å,°] of the optimized structures of key species for allylic **5s**⇌**5a** isomerization. The cutoff for drawing Nd–C bonds was arbitrarily set to 3.1 Å. The hydrogen atoms on the methyl groups of the catalyst backbone are omitted for the sake of clarity.

as determined experimentally for related (η^3-allyl)$_3$La complexes.[14b,d,26] Excess amine substrate can reasonably be imagined to stabilize the $\eta^1(C^3)$-allylic TS_{ISO}[**5**] and thus facilitate the isomerization kinetically. In fact, the TS_{ISO}[**5**]-AS adduct (Figure S4, Supporting Information) becomes 7.3 kcal mol^{-1} lower in enthalpy relative to TS_{ISO}[**5**] ($\Delta\Delta H^{\neq}$, Table 3), which, however, is approximately equivalent to the entropic disfavor caused by amine complexation. As a result, very similar kinetics are predicted in terms of free energy, regardless of whether the step is assisted by excess amine substrate or not. This indicates this step to be kinetically more expensive, and thus slower, than intermolecular insertion (see above) and ensuing protonolysis (see below).

Protonolysis of the η^3-butenyl-amine–Nd intermediate: Following the various insertion pathways that afford **5s**, **5a**, and **6t**, **6c**, respectively, ensuing protonolysis by **1** gives rise to aminoalkene-amido–Nd compounds **7** and **8** (Scheme 2), from which the aminoalkene products are liberated in a facile substitution by **1**, which initiates a new catalytic cycle by regeneration of **3**. It was shown in Section I.B that the insertion step proceeds with complete regioselectivity by following exclusively the 1,4-path. As a consequence, first, **8** has a negligible population and, second, the **6**+**1**→**8** (+**1**)→**10** (+**3**-AS) path for generation of branched aminoalkenes remains closed, irrespective of whether protonolysis is kinetically affordable or not. Therefore, this section focuses exclusively on the alternative pathways for protonolysis of **5s**, **5a** by **1**, for which structural and energy data are presented in Figure 4 and Table 4, respectively.

The two reactive carbon atoms of the butenyl moiety in **5** are both eligible for protonation. From substituted C^3 in **5s**, **5a**, first **7c**, **7d** are generated, from which rotamers **9c**, **9d** of *N*-(3-butenyl)-*n*-propylamine, respectively, are subsequently liberated. The regioisomeric pathways for proton transfer to the terminal, unsubstituted carbon atom C^1 afford **7a**, **7b** and successively *trans*-2- and *cis*-2-butenyl isomers **9a**, **9b** of *N*-(2-butenyl)-*n*-propylamine, respectively, when commencing from **5s** and **5a**. For the initial formation of precursor species **5s**-AS and **5a**-AS, incoming substrate **1** must compete for coordination with η^3-butenyl and tethered η^1-N-amine moieties, and this leads to a more relaxed coordination sphere in the amine adducts when compared to **5s**, **5a**. As far as the **7a**-, **7b**-generating pathways are concerned, the η^3-π mode of the butenyl–Nd coordination is retained in the adducts[27] together with an intact η^1-N complexation of the tethered amine in **5a**-AS, which, however, is cleaved in **5s**-AS (Figure 4). For protonation of C^3, however, the *cis*-approaching **1** displaces the tethered amino group from the immediate proximity of the Nd atom. Amine uptake is predicted to range from a slightly exothermic to a thermoneutral process (ΔH, Table 4). Among the precursors for C^1/C^3 protonation the one involved in the **7c**-, **7d**-generating pathways (Figure 4) are slightly favorable owing to relief of steric congestion around the lanthanide.

A σ-bond metathesis-type transition-state structure, representing simultaneous N–H bond cleavage and C–H bond formation in the proximity of the Nd center, is encountered along the minimum-energy path for each of the various protonolysis pathways and is characterized by partial allyl→vinyl transformation (Figure 4). Starting from a η^3-butenyl-Nd moiety in **5s**-AS and **5a**-AS, the C^1 and C^3 carbon atoms that undergo protonation are displaced from the immediate proximity of the Nd atom while traversing through the transition state. This reduction of the coordination number around Nd is compensated for in TS[5-AS–**7a**] and TS[**5a**-AS–**7b**] by a recoordinating and closer approaching, respectively, chelating amine tether group (Figure 4). In contrast, this supporting influence is not operative along the pathways for C^3 protonolysis, as here the two *cis*-disposed amine moieties prevent any effective tether-amine–Nd interactions. Following the reaction path further, passage through the transition state leads to **7a**, **7b** and **7c**, **7d**, in which the aminoalkene is coordinated through its N-donor center and olefin double bond, respectively, to Nd in the initially formed product species.

The predicted energy profile for the various pathways reflects the structural aspects. Of the two regioisomeric paths, proton transfer to the butenyl C^1 carbon atom is more feasible kinetically and is also driven by a stronger thermodynamic force (Table 4), which has its primary origin in the supporting influence of the chelating amine tether group (see above). The alternative protonation of the substituted butenyl C^3 carbon atom via **5s**/**5a**+**1**→**7c**/**7d** is predicted to be distinctly impeded by both kinetic and thermodynamic factors. These steps are endergonic (ΔG = 7.7–10.4 kcal mol^{-1}) and require a significant total barrier of 19.5–20.3 kcal mol^{-1} ($\Delta G^{\neq}$, relative to {**5s**+**1**}) to be overcome.

Of the two stereoisomeric **5s**+**1**→**7a** and **5a**+**1**→**7b** pathways, **5s** exhibits a higher propensity to undergo protonolysis, which is linked to a total free energy of activation of 14.1 kcal mol^{-1}. The competing **7b**-generating pathway, however, has a total barrier of 17.7 kcal mol^{-1} ($\Delta G^{\neq}$). Subsequent expulsion of the aminoalkene products through **7a**/**7b**+**1**→**3**-AS+**9a**/**9b** is a highly facile,[28] thus instantaneously occurring, exergonic process (ΔG = −7.1/−7.1 kcal mol^{-1}), which drives the overall **5a**/**5s**+**1**→**7a**/**7b** (+**1**)→**9a**/**9b** (+**3**-AS) process downhill. Overall, 1) generation of **7a**/**9a** is predicted to be energetically most feasible among the various pathways, which 2) occurs in an irreversible fashion and 3) is associated with a large negative activation entropy ($\Delta S^{\neq}$ = −29.2 e.u., Table 4) that is essentially due to initial amine-adduct formation.

Finally, the possible assistance of protonolysis by excess substrate **1** was computationally explored. Two borderline cases are imaginable, in which the amine can act, first, as a passive spectator ligand or, second, as a "proton shuttle", that is, an active mediator. Having already probed the second alternative for the first precatalyst activation, we decided to focus here on the first case. To this end, the full set of transition states TS[**5**-AS–**7**]-AS for the various pathways that commence from **5** were located with **1** as amine substrate (Figure S5, Supporting Information), while the kinetics are included in Table 4. For the favorable proton transfer

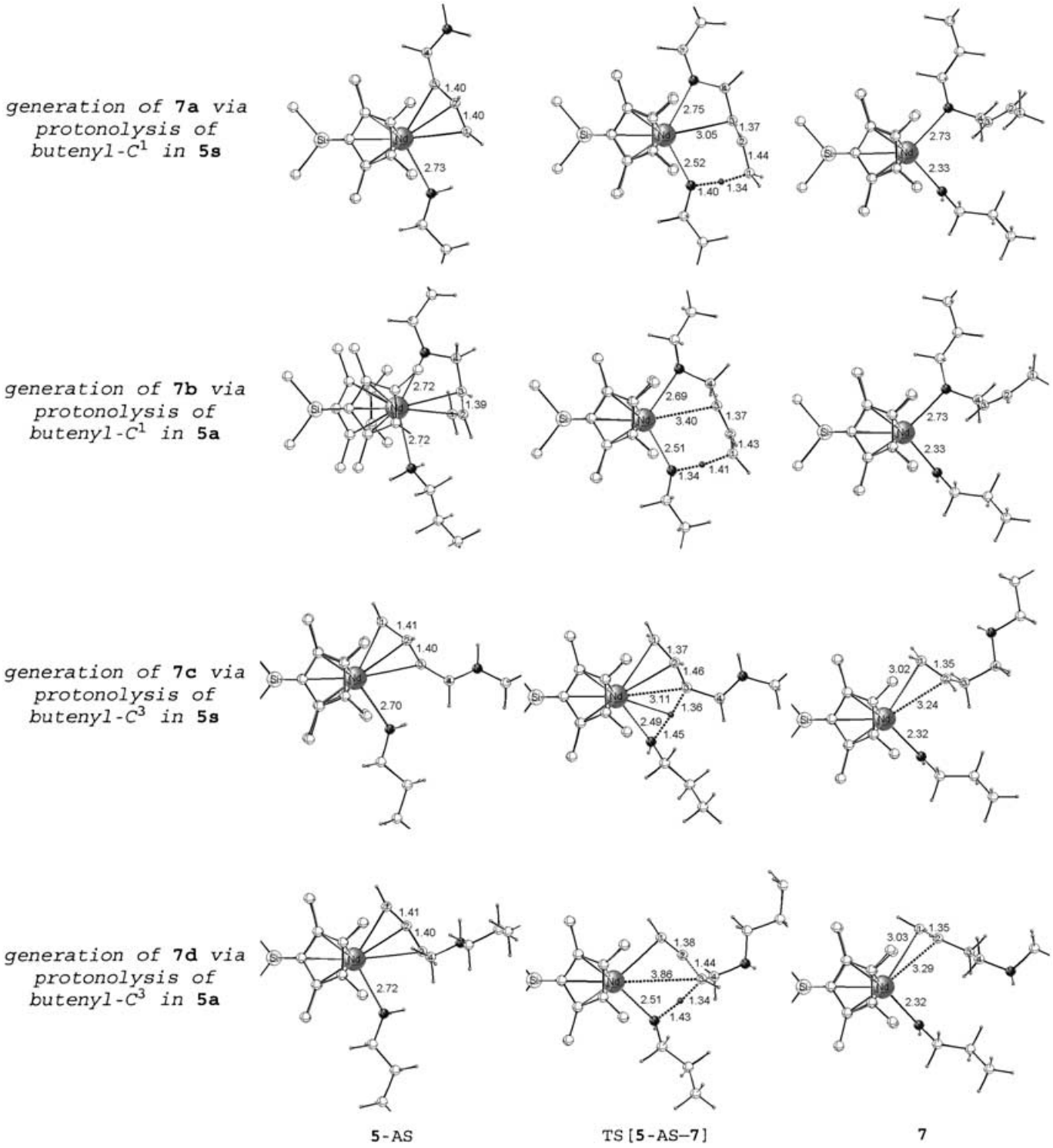

Figure 4. Selected geometric parameters [Å] of the optimized structures of key species for protonolysis of the η^3-butenyl–Nd complex **5** by amine substrate **1** (AS) affording aminoalkene-amido–Nd compounds **7a**–**7d** along alternative pathways. The cutoff for drawing Nd−C bonds was arbitrarily set to 3.1 Å. Several of the species are displayed in truncated fashion. The hydrogen atoms on the methyl groups of the catalyst backbone are omitted for the sake of clarity.

to C^1 only a small enthalpic stabilization of the transition states upon additional amine complexation is predicted ($\Delta\Delta H^{+} = 0.2/4.0$ kcal mol^{-1} for **7a**/**7b**-generating pathways). Thus, in terms of free energy, excess amine does not facilitate the favorable protonolysis pathway kinetically, and is therefore not likely to assist this process. As anticipated, a significant acceleration is predicted for the **7c**/**7d**-production pathways on the ΔH surface due to compensation of the

Table 4. Enthalpies and free energies of activation and reaction for protonolysis of the η^3-allyl-Nd intermediate **5** by amine substrate **1** to afford the aminoalkene-amido–Nd compounds **7a–d** along various regioisomeric pathways for H transfer (H-trf).[a,b]

Insertion pathway	**5**-AS[c]	Aminoalkene-generating pathway TS	**7**[c]
1,4-insertion			
7a/9a via H-trf to C^1 of **5s**	−3.2/*3.8* (**5s**-AS)	5.4/*14.1* ($\Delta S^{\ddagger}=-29.2$ e.u.)[d]	*N*-(*trans*-2-butenyl)-*n*-propylamine (**7a**) −8.3/*−1.3*
7b/9b via H-trf to C^1 of **5a**	0.1/*7.9* (**5a**-AS)	9.1/*17.7* ($\Delta S^{\ddagger}=-28.9$ e.u.)[d]	*N*-(*cis*-2-butenyl)-*n*-propylamine (**7b**) −6.8/*0.2*
7c/9c via H-trf to C^3 of **5s**	−4.5/*2.9* (**5s**-AS)	12.1/*19.5* ($\Delta S^{\ddagger}=-25.0$ e.u.)[d]	*N*-(*3E*-butenyl)-*n*-propylamine (**7c**) 1.1/*7.7*
7d/9d via H-trf to C^3 of **5a**	−0.9/*6.4* (**5a**-AS)	12.8/*20.3* ($\Delta S^{\ddagger}=-25.3$ e.u.)[d]	*N*-(*3Z*-butenyl)-*n*-propylamine (**7d**) 3.8/*10.4*
insertion pathway		amine-substrate-assisted aminoalkene-generating pathway[e] TS	
1,4-insertion			
7a/9a via H-trf to C^1 of **5s**		5.2/*22.2*	
7b/9b via H-trf to C^1 of **5a**		5.1/*21.6*	
7c/9c via H-trf to C^3 of **5s**		4.4/*20.4*	
7d/9d via H-trf to C^3 of **5a**		6.0/*21.9*	

[a] Total barriers, reaction energies, and activation entropies are relative to {**5s**+**1**}. [b] Activation enthalpies and free energies ($\Delta H^{\ddagger}/\Delta G^{\ddagger}$) and reaction enthalpies and free energies ($\Delta H/\Delta G$) are given in kilocalories per mole; values in italic type are the Gibbs free energies. [c] See text (or Scheme 2) for description of the various isomers of the amine adduct **5**-AS and product complex **7**. [d] The activation entropy is given in entropic units (cal mol^{-1} K^{-1}). [e] The process assisted by an additive amine molecule was investigated for **1** as amine substrate (AS), which acts as a Nd-coordinated spectator ligand. Total barriers, reaction energies, and activation entropies are relative to {**5s**+2×**1**}.

lacking tether-amine–Nd interaction (see above) by coordination of **1**. The computed enthalpic stabilization on amine complexation is of the same magnitude as the associated entropic costs. Hence, these pathways may benefit from association of an additive amine molecule, which, however, affects the kinetics to only a small extent. As a consequence, the **7c**/**7d**-generating pathways are still distinctly separated by a gap greater than 6 kcal mol^{-1} ($\Delta\Delta G^{\ddagger}$) relative to the favorable **7a**-generating pathway, and are therefore not accessible and have no relevance for any further mechanistic considerations.

Catalytic reaction course of intermolecular hydroamination of 1,3-dienes and primary amines

Gibbs free-energy profile: The Gibbs free-energy profile of all critical elementary steps of the tentative catalytic cycle (Scheme 2) is presented in Scheme 3, which comprises solely viable pathways. More detailed enthalpy and free-energy profiles (Schemes S1, S2) can be found in the Supporting Information. Scheme 3, together with the detailed insight into individual steps revealed in previous sections, brings us to a position where we can complement experiments with regard to deeper understanding of general aspects of organolanthanide-mediated

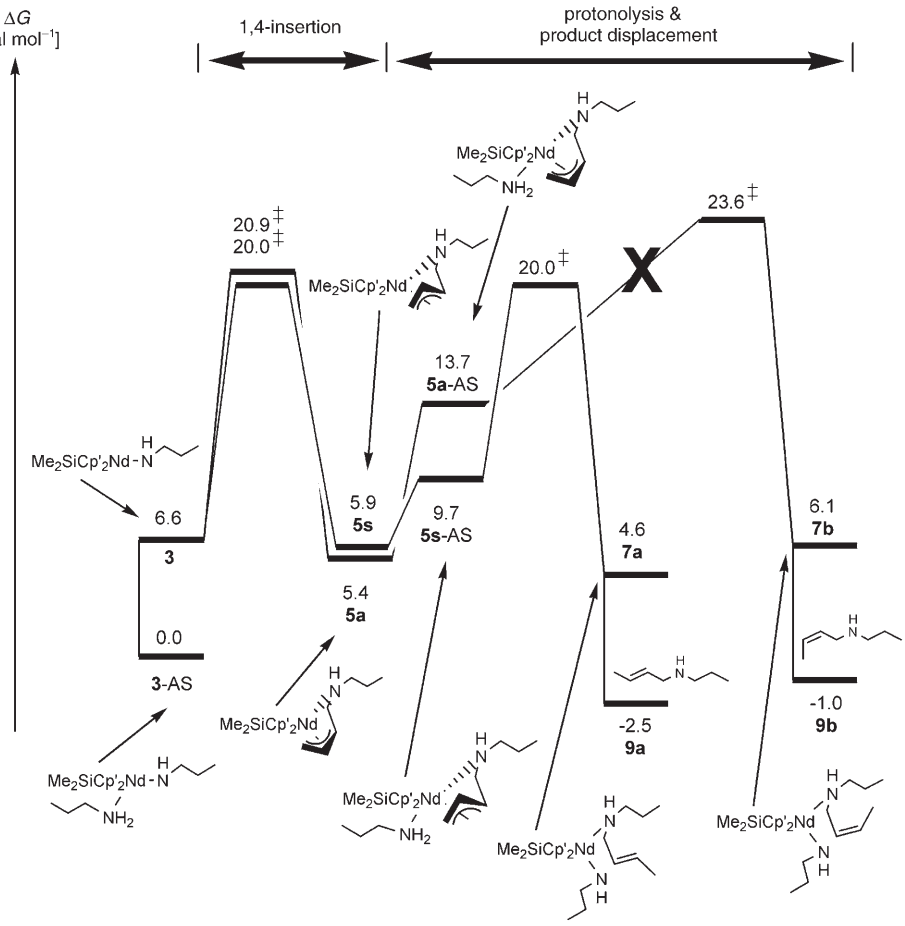

Scheme 3. Condensed Gibbs free-energy profile [kcal mol^{-1}] of the intermolecular hydroamination of 1,3-butadiene and *n*-propylamine (**1**) mediated by [$Me_2SiCp'_2NdCH(TMS)_2$] precatalyst **2**. Only the most feasible pathways for individual steps are included, while alternative, but unfavorable pathways are omitted for the sake of clarity (see also Scheme S2, Supporting Information). Aminoalkene displacement through **7a**/**7b**+**1**→**3**-AS+**9a**/**9b** is included.

intermolecular hydroamination by unraveling the salient features of 1,3-diene intermolecular hydroamination. A detailed kinetic study has, unfortunately, not been reported for this process thus far. The following conclusions can be drawn: 1) The **3**-AS adduct is predicted to be the prevalent species of the catalytic cycle and thus likely represents the catalyst's resting state under actual reaction conditions.[9c,29] 2) C–N bond formation by butadiene insertion into the Nd–N bond necessitates displacement of the amine from **3**-AS to form the catalytically active complex **4**. The present computational study provides no indication for the favorable 1,4-insertion path being facilitated by excess reactants, either by butadiene or by **1**. 3) Ensuing protonolysis of **5** by incoming amine **1** to afford linear aminoalkene products is also not likely to be assisted by additive reactant molecules. 4) C–N bond formation along **3**+*trans*/*cis*-C_4H_6→**5s**/**5a** and subsequent protonolysis by **5s**/**5a**+**1**→**7a**/**7b** are the crucial steps that determine the activity and selectivity of hydroamination. Alternative pathways for these steps, as well as **5s**⇔**5a** allylic isomerization, are predicted to be significantly more difficult kinetically and therefore not accessible under actual reaction conditions. Furthermore, **7a**+**1**→**3**-AS+**9a** product displacement is a highly facile, hence instantaneously occurring, exergonic process. 5) Identical total free-energy barriers[30] are predicted for the most feasible **3**+*trans*-C_4H_6→**5s** and **5s**+**1**→**7a** pathways of the two bimolecular insertion and protonolysis steps. Butadiene insertion is driven by a small thermodynamic force of only -0.7 kcal mol^{-1} (ΔG), and hence is likely to occur in a reversible fashion. In contrast, **5s**+**1**→**7a** (+**1**)→**9a** (+**3**-AS) protonolysis linked to immediate product release is downhill ($\Delta G = -8.4$ kcal mol^{-1}).

Although it is not possible to predict the turnover-limiting step from the computed free-energy profile, we suggest the mechanistic scenario outlined in Scheme 4 for the organolanthanide-supported intermolecular hydroamination of 1,3-dienes. This scenario consists of kinetically mobile, reversible amine association/dissociation in **3** (K_1) and **5s** (K_4) and 1,3-diene association in **3** (K_2), C–C insertion into the Nd–N bond (k_3) and ensuing turnover-limiting protonolysis ($k_5 \equiv k_{prod}$). Starting from the resting state **3**-AS, the amine must first dissociate before **3** can accommodate incoming 1,3-diene to lead first to the catalytically active species **4**-1,4t and subsequently give rise to **5s** after feasible 1,4-insertion (k_3), which is likely to be reversible. The entropic contributions for the dissociative/associative equilibria K_1, K_2 approximately cancel each other, so that the insertion step, although bimolecular, is associated with only a small negative total reaction entropy ($\Delta S_{tot} = -6.5$ e.u.).[30] On the other hand, bimolecular proton transfer is characterized by a large negative activation entropy of -29.2 e.u. (Table 4), the majority of which originates from the association equilibrium K_4 ($\Delta S = -23.6$ e.u.). Kinetic analysis assuming kinetically mobile equilibria K_1, K_2, K_4 and applying steady-state concentrations for **5s**,[31] which can reasonably be assumed to occur in negligible stationary concentrations (see above), yields the rate law of Equation (2).[32] This law predicts first-order behavior in [catalyst] and [diene],[33] and thus is in general agreement with the empirical law in Equation (1), derived from experiment.[9a,b]

$$\text{velocity} = K_1K_2K_4k_3k_5[\text{diene}][\mathbf{3}\text{-AS}]k_4[\text{AS}]^{-1} \qquad (2)$$

Although amine reactant is involved in the turnover-limiting protonolysis, the kinetics are nevertheless zeroth-order in [amine] owing to the associated dissociation/association equilibria K_1 and K_4. For this mechanistic scenario, an effective total enthalpy barrier of 11.3 kcal mol^{-1} ($\Delta H^{\pm}_{tot}$)[29,30] is predicted for the most feasible **7a**-generating pathway for protonolysis (Scheme S1, Supporting Information), which is connected with an estimated negative total activation entropy of -35.7 e.u. ($\Delta S^{\pm}_{tot}$).[30] Thus the computationally predict-

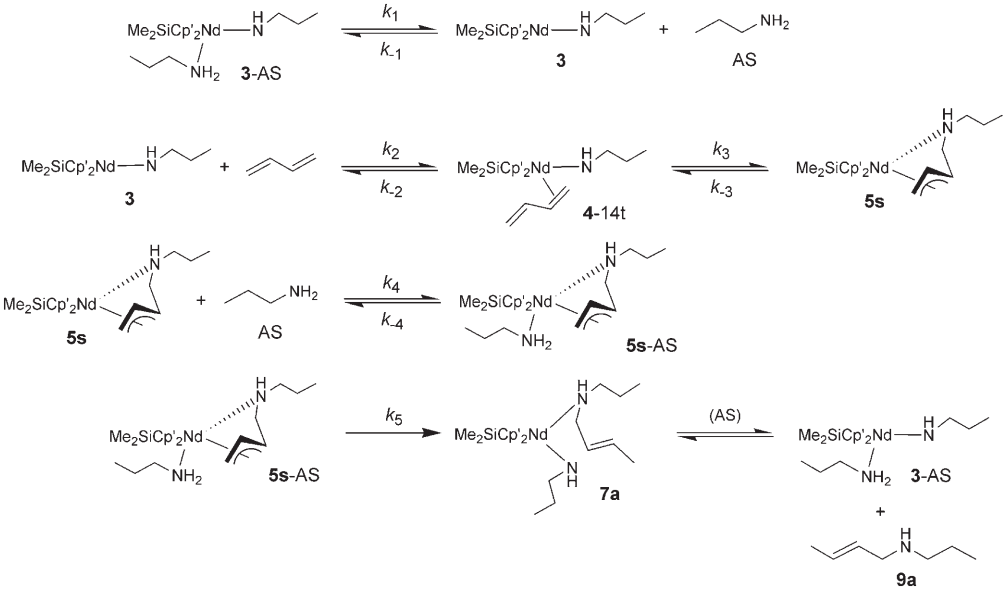

Scheme 4. Proposed mechanistic scenario for the organolanthanide-mediated intermolecular hydroamination of 1,3-dienes and primary amines.

ed kinetics are in reasonable agreement with experimental data for alkyne intermolecular hydroamination.[15] The large negative value for $\Delta S^{\neq}_{tot}$ originates primarily from amine association via K_4 and, to smaller extents, from ΔS for butadiene insertion (k_3) and $\Delta S^{\neq}$ for turnover-limiting protonolysis (k_5). The entropy contributions for equilibria K_1, K_2, however, essentially compensate each other. The proposed mechanistic scenario (Scheme 4) in combination with the computed free-energy profile (Schemes 3 and S2) is consistent with the empirical rate law [Eq. (1)] and accounts for crucial experimental observations.[9]

The computationally verified mechanistic scenario for the organolanthanide-mediated intermolecular hydroamination of 1,3-dienes contrasts with the general mechanism proposed by Marks et al.,[7,9a,b] who suggested insertion of unsaturated C–C bonds into the Ln–N bond as being turnover-limiting for the various unsaturated C–C functionalities.[9d] This alternative scenario with 1,4-insertion as the turnover-controlling step (i.e., $k_3 \equiv k_{prod}$) would give rise to a rate law[34] that predicts first-order dependence on [catalyst] and [diene]. This rate law is equally as consistent with the empirical rate law [Eq. (1)] as Eq. (2) is. The following kinetics can be deduced from the computed energy profiles:[35] $\Delta H^{\neq}_{tot} = 20.7$ kcal mol^{-1}, $\Delta S^{\neq}_{tot} = -4.2$ e.u. The small $\Delta S^{\neq}_{tot}$ value (see above), however, is in sharp contrast with the experimentally measured large negative activation entropy[15] and therefore rules this mechanistic scenario out.

Factors governing regioselectivity and double-bond selectivity: This section elucidates the factors that discriminate between the various pathways for insertion and protonolysis and thereby govern the issues of regio- and stereoselectivity of 1,3-diene intermolecular hydroamination. The C–N bond-forming step is the crucial step that determines whether linear or branched aminoalkene products are formed. The 1,4-insertion path is predicted by both kinetic ($\Delta\Delta G^{\neq} = 7.3$ kcal mol^{-1})[36] and thermodynamic ($\Delta\Delta G = 13.2$ kcal mol^{-1})[36] factors (see Section I.B) to be distinctly preferred over the regioisomeric 1,2-path, and hence this process occurs with complete regioselectivity. This rationalizes the exclusive formation of linear (i.e., 1,4-insertion) products that is observed by experiment.[9] The strong preference for traversing through the **3**+C_4H_6→**5** path has its primary origin in the coordinative assistance of the TS and product species by the emerging and established η^3-butenyl–Nd interaction, respectively. With regard to the stereoselectivity, almost identical free-energy profiles are predicted for the alternative *trans*-1,4 and *cis*-1,4 pathways, which should therefore be passed through with similar probabilities.

Accordingly, precursors **5s**, **5a** for protonolysis are present in comparable concentration, but they do not occur in rapid equilibrium. Isomerization of the η^3-butenyl–Nd group in **5** is connected with a significant barrier ($\Delta G^{\neq} = 18.2$ kcal mol^{-1}), and is thus slow and kinetically retarded relative to ensuing protonolysis that follows the most feasible pathway ($\Delta\Delta G^{\neq} = 4.1$ kcal mol^{-1}). This indicates that **5s**⇌**5a** interconversion is almost suppressed and plays no role in selectivity control. The distribution of the various linear aminoalkenes **9a**–**9d** is entirely regulated kinetically by the aptitude of the equally populated precursor **5s**, **5a** to traverse through the competing pathways for protonolysis.

Proton transfer to the terminal butenyl C^1 carbon atom in **5** is the dominant path for protonolysis, while the regioisomeric path for C^3 protonation is distinctly more difficult kinetically ($\Delta\Delta G^{\neq} = 5.4$ kcal mol^{-1})[36] and also less favorable thermodynamically ($\Delta\Delta G = 9.0$ kcal mol^{-1}),[36] as the former path benefits from coordinative assistance of the chelating amine tether functionality (see Section I.D). The predicted kinetic gap can be considered large enough to completely prevent production of *N*-(3-butenyl)-*n*-propylamine. Among the alternative **5s**/**5a**+**1**→**7a**/**7b** (+**1**)→**9a**/**9b** (+**3**-AS) pathways, the *syn*-η^3-butenyl–Nd form **5s** exhibits a higher propensity to undergo proton transfer ($\Delta\Delta G^{\neq} = 3.6$ kcal mol^{-1}); thus, the **9a**-generating pathway is predicted to be kinetically easiest among the various pathways. Accordingly, protonolysis of the exclusively formed 1,4-insertion compound **5** occurs with almost complete stereoselectivity and affords *N*-(*trans*-2-butenyl)-*n*-propylamine (**9a**) as sole aminoalkene product, while the pathways towards alternative product isomers are entirely precluded kinetically due to associated activation barriers that are distinctly higher. This conforms to the experimentally observed product composition[9] and rationalizes furthermore the regio- and stereochemical outcome of the intermolecular hydroamination of 1,3-butadiene with primary amines.

Concluding Remarks

Herein is presented, to the best of my knowledge, the first comprehensive computational mechanistic exploration of the entire catalytic reaction course for the organolanthanide-catalyzed intermolecular hydroamination of 1,3-dienes and primary amines by a prototypical *ansa*-neodymocene-based catalyst. All critical elementary processes for a tentative catalytic cycle (Scheme 2) have been scrutinized in terms of structural and energetic aspects by means of a reliable gradient-corrected DFT method for the experimentally studied intermolecular hydroamination of 1,3-butadiene and *n*-propylamine (**1**) mediated by the real [$Me_2Si(\eta^5$-$Me_4C_5)_2NdCH(SiMe_3)_2$] precatalyst **2**. The present computational investigation provides a detailed insight, first, into general mechanistic aspects of organolanthanide-mediated intermolecular hydroamination and, second, into the salient features of the intermolecular hydroamination of 1,3-dienes. This study therefore complements experiments with regard to a deeper understanding and rationalization of the experimental results and should assist the rational design of new catalysts.

The enhanced insights revealed by the present study can be summarized as follows: 1) Precatalyst activation is predicted to occur in an almost quantitative fashion through kinetically facile, strongly exergonic protonolysis by amine **1** to give the amido–Nd complex **3**. 2) This compound is pre-

dominantly present under actual reaction conditions as amine adduct **3**-AS, which most likely represents the catalyst's resting state. 3) The amine must first dissociate from **3**-AS before incoming butadiene can coordinate to the Nd center and subsequently insert into the Nd–amido bond. C–N bond formation occurs with complete regioselectivity, passing exclusively through the 1,4-path. This process does not benefit from the coordinative assistance of either excess amine or 1,3-diene reactants. The stereoisomeric *trans*-1,4 and *cis*-1,4 insertion pathways are characterized by very similar energy profiles, which indicates that they occur with comparable probabilities. 4) Accordingly, the precursor species **5s**, **5a** for ensuing protonolysis are present in similar populations, but they are not in rapid equilibrium. The **5s**⇌**5a** conversion is kinetically disabled relative to protonolysis, so allylic isomerization does not play any role in control of selectivity. The selectivity for the aminoalkene product is entirely regulated kinetically by the abilities of **5s**, **5a** to follow the various protonolysis pathways. 5) The two reactive sites of the η^3-butenyl–Nd moiety are predicted to exhibit distinctly different propensities for protonation, and this explains the almost complete regioselectivity of the proton-transfer process. The coordinative assistance of the chelating amine tether, but not of additive amine molecules, makes proton transfer to the terminal, unsubstituted butenyl C^1 atom the path that is almost entirely passed through. Following this path, protonolysis of **5s** (i.e., the *trans*-1,4 insertion product) is significantly less expensive kinetically compared to **5a** and affords *N*-(*trans*-2-butenyl)-*n*-propylamine (**9a**) as sole product. This rationalizes the experimentally observed regio- and stereoselectivity. 6) A computationally verified, mechanistic scenario comprising kinetically mobile reactant association/dissociation equilibria and facile, reversible intermolecular diene insertion into the Nd–amido bond, linked to turnover-limiting protonolysis of the η^3-butenyl–Nd functionality, has been suggested (Scheme 4). The refined mechanistic scenario, which revises prior mechanistic assumptions, in combination with the computed free-energy profile is consistent with the empirical rate law [Eq. (1)] and accounts for crucial experimental observations.[9,15] Whether this mechanism can be generalized to organolanthanide-assisted intermolecular hydroamination of the various other unsaturated C–C functionalities will be the subject of forthcoming investigations.

Acknowledgements

I wish to thank Professor Tom Ziegler (University of Calgary, Canada) for his generous support. Excellent service by the computer centers URZ Halle and URZ Magdeburg is gratefully acknowledged.

[1] For reviews of catalytic hydroamination, see a) R. Taube in *Applied Homogeneous Catalysis with Organometallic Complexes* (Eds.: B. Cornils, W. A. Herrmann), Wiley-VCH, Weinheim, **1996**, pp. 507–520; b) L. S. Hegedus, *Angew. Chem.* **1988**, *100*, 1147; *Angew. Chem. Int. Ed. Engl.* **1988**, *27*, 1113; c) D. M. Roundhill, *Catal. Today* **1997**, *37*, 155; d) T. E. Müller, M. Beller, *Chem. Rev.* **1998**, *98*, 675; e) J. J. Brunet, D. Neibecker in *Catalytic Heterofunctionalization* (Eds.: A. Togni, H. Grützmacher), Wiley-VCH, Weinheim, **2001**, pp. 91–141; f) M. Nobis, B. Drießen-Hölscher, *Angew. Chem.* **2001**, *113*, 4105; *Angew. Chem. Int. Ed.* **2001**, *40*, 3983; g) F. Pohlki, S. Doye, *Chem. Soc. Rev.* **2003**, *32*, 104; h) P. W. Roesky, T. E. Müller, *Angew. Chem.* **2003**, *115*, 2812; *Angew. Chem. Int. Ed.* **2003**, *42*, 2708; i) J. F. Hartwig, *Pure Appl. Chem.* **2004**, *76*, 507.

[2] For hydroamination mediated by early transition metals, see: a) P. L. McGrane, M. Jensen, T. Livinghouse, *J. Am. Chem. Soc.* **1992**, *114*, 5459; b) P. L. McGrane, T. Livinghouse, *J. Org. Chem.* **1992**, *57*, 1323; c) P. L. McGrane, T. Livinghouse, *J. Am. Chem. Soc.* **1993**, *115*, 11485; d) D. Fairfax, M. Stein, T. Livinghouse, M. Jensen, *Organometallics* **1997**, *16*, 1523; e) F. Pohlki, S. Doye, *Angew. Chem.* **2001**, *113*, 2361; *Angew. Chem. Int. Ed.* **2001**, *40*, 2305; f) J. S. Johnson, R. G. Bergmann, *J. Am. Chem. Soc.* **2001**, *123*, 2923; g) C. Cao, J. T. Ciszewski, A. L. Odom, *Organometallics* **2001**, *20*, 5011; h) L. Ackermann, R. G. Bergmann, *Org. Lett.* **2002**, *4*, 1475; i) T.-G. Ong, G. P. A. Yap, D. S. Richeson, *Organometallics* **2002**, *21*, 2839; j) A. Tillack, I. G. Castro, C. G. Hartung, M. Beller, *Angew. Chem.* **2002**, *114*, 2646; *Angew. Chem. Int. Ed.* **2002**, *41*, 2541; k) Y. Shi, C. Hall, J. T. Ciszewski, C. Cao, A. L. Odom, *Chem. Commun.* **2003**, 586.

[3] For hydroamination mediated by late transition metals, see: a) T. E. Müller, M. Grosche, E. Herdtweck, A.-K. Pleier, E. Walter, Y.-K. Yan, *Organometallics* **2000**, *19*, 170; b) D. Vasen, A. Salzer, F. Gerhards, H.-J. Gais, R. Stürmer, N. H. Bieler, A. Togni, *Organometallics* **2000**, *19*, 539; c) M. Kawatsura, J. F. Hartwig, *Organometallics* **2001**, *20*, 1960; d) T. E. Müller, M. Berger, M. Grosche, E. Herdtweck, F. P. Schmidtchen, *Organometallics* **2001**, *20*, 4384; e) C. G. Hartung, A. Tillack, H. Trauthwein, M. Beller, *J. Org. Chem.* **2001**, *66*, 6339; f) U. Nettekoven, J. F. Hartwig, *J. Am. Chem. Soc.* **2002**, *124*, 1166; g) V. Neff, T. E. Müller, J. A. Lecher, *Chem. Commun.* **2002**, 906; h) L. Fadini, A. Togni, *Chem. Commun.* **2003**, 30.

[4] For hydroamination mediated by rare earth metals, see: a) M. R. Gagné, T. J. Marks, *J. Am. Chem. Soc.* **1989**, *111*, 4108; b) M. R. Gagné, C. L. Stern, T. J. Marks, *J. Am. Chem. Soc.* **1992**, *114*, 275; c) Y. Li, T. J. Marks, *J. Am. Chem. Soc.* **1996**, *118*, 9295; d) G. A. Molander, E. D. Dowdy, *J. Org. Chem.* **1998**, *63*, 8983; e) Y. Li, T. J. Marks, *J. Am. Chem. Soc.* **1998**, *120*, 1757; f) V. M. Arredondo, F. E. McDonald, T. J. Marks, *Organometallics* **1999**, *18*, 1949; g) V. M. Arredondo, S. Tian, F. E. McDonalds, T. J. Marks, *J. Am. Chem. Soc.* **1999**, *121*, 3633; h) Y. K. Kim. T. Livinghouse, J. E. Bercaw, *Tetrahedron Lett.* **2001**, *42*, 2933; i) Y. K. Kim, T. Livinghouse, *Angew. Chem.* **2002**, *114*, 3797; *Angew. Chem. Int. Ed.* **2002**, *41*, 3645; j) J. Wang, A. K. Dash, M. Kapon, J.-C. Berthet, M. Ephritikhine, M. S. Eisen, *Chem. Eur. J.* **2002**, *8*, 5384; k) Y. K. Kim, T. Livinghouse, Y. Horino, *J. Am. Chem. Soc.* **2003**, *125*, 9560; l) D. V. Gribkov, K. C. Hultzsch, F. Hampel, *Chem. Eur. J.* **2003**, *9*, 4796; m) B. D. Stubbert, C. L. Stern, T. J. Marks, *Organometallics* **2003**, *22*, 4836; n) J.-S. Ryu, T. J. Marks, F. E. McDonald, *J. Org. Chem.* **2004**, *69*, 1038; o) F. Lauterwasser, P. G. Hayes, S. Bräse, W. E. Piers, L. L. Schafer, *Organometallics* **2004**, *23*, 2234; p) K. C. Hultzsch, F. Hampel, T. Wagner, *Organometallics* **2004**, *23*, 2601.

[5] For reviews on organolanthanides, see: a) T. J. Marks, R. D. Ernst in *Comprehensive Organometallic Chemistry* (Eds.: G. Wilkinson, F. G. A. Stone, E. W. Abel), Pergamon Press, Oxford, **1982**, Chap. 21; b) W. J. Evans, *Adv. Organomet. Chem.* **1985**, *24*, 131; c) C. J. Schaverien, *Adv. Organomet. Chem.* **1994**, *36*, 283; d) H. Schumann, J. A. Meese-Marktscheffel, L. Esser, *Chem. Rev.* **1995**, *95*, 865; e) F. T. Edelmann in *Comprehensive Organometallic Chemistry, Vol. 4* (Eds.: G. Wilkinson, F. G. A. Stone, E. W. Abel), Pergamon Press, Oxford, **1995** Chap. 2; f) M. N. Bochkarev, *Chem. Rev.* **2002**, *102*, 2089; g) S. Arndt, J. Okuda, *Chem. Rev.* **2002**, *102*, 1953; h) F. T. Edelmann, D. M. M. Freckmann, H. Schumann, *Chem. Rev.* **2002**, *102*, 1851; i) H. C. Aspinall, *Chem. Rev.* **2002**, *102*, 1807.

[6] For reviews on organolanthanide catalysis, see: a) G. Jeske, H. Lauke, H. Mauermann, H. Schumann, T. J. Marks, *J. Am. Chem. Soc.* **1985**, *107*, 8111; b) P. L. Watson, G. W. Parshall, *Acc. Chem. Res.* **1985**, *18*, 51; c) H. J. Heeres, J. Renkema, M. Booji, A. Meetsma, J. H. Teuben, *Organometallics* **1988**, *7*, 2495; d) G. A. Moland-

er, J. O. Hoberg, *J. Org. Chem.* **1992**, *57*, 3266; e) P. J. Shapiro, W. D. Cotter, W. P. Schaefer, J. A. Labinger, J. E. Bercaw, *J. Am. Chem. Soc.* **1994**, *116*, 4623; f) P.-F. Fu, L. Brard, Y. Li, T. J. Marks, *J. Am. Chem. Soc.* **1995**, *117*, 7157; g) F. T. Edelmann, *Top. Curr. Chem.* **1996**, *179*, 247; h) G. A. Molander, *Chemtracts: Org. Chem.* **1988**, *18*, 237; i) *Topics in Organometallic Chemistry*, *Vol. 2* (Ed.: S. Kobayashi), Springer, Berlin, **1999**; j) Z. Hou, Y. Wakatsuki, *Coord. Chem. Rev.* **2002**, *231*, 1; k) G. A. Molander, J. A. C. Romero, *Chem. Rev.* **2002**, *102*, 2161; l) M. Shibasaki, N. Yoshikawa, *Chem. Rev.* **2002**, *102*, 2187; m) J. Inanaga, H. Furuno, T. Hayano, *Chem. Rev.* **2002**, *102*, 2211.

[7] S. Hong, T. J. Marks, *Acc. Chem. Res.* **2004**, *37*, 673.

[8] a) S. Hong, T. J. Marks, *J. Am. Chem. Soc.* **2002**, *124*, 7886; b) S. Hong, A. M. Kawaoka, T. J. Marks, *J. Am. Chem. Soc.* **2003**, *125*, 15878; c) S. Hong, S. Tian, M. V. Metz, T. J. Marks, *J. Am. Chem. Soc.* **2003**, *125*, 14768.

[9] a) Y. Li, T. J. Marks, *Organometallics* **1996**, *15*, 3770; b) J.-S. Ryu, G. Y. Li, T. J. Marks, *J. Am. Chem. Soc.* **2003**, *125*, 12584. c) Typical reaction conditions for the stereoselective organolanthanide-mediated intermolecular hydroamination of 1,3-dienes with primary amines are 49- and 29-fold molar excess of 1,3-butadiene and *n*-propylamine (**1**) reactants, respectively, together with the precatalyst (e.g., $[Me_2SiCp'_2NdCH(TMS)_2]$ (**2**) at 60 °C in benzene. Only the *trans*-1,4 addition product (i.e., **9a**) was detected by ^{1}H NMR spectroscopy; detailed kinetics, however, were not reported. d) Intermolecular hydroamination has been established for a variety of unsaturated C–C functionalities, namely, alkenes, alkynes, vinylarenes, 1,3-dienes, and methylenecycloalkanes.[7, 9a,b]

[10] a) M. Kawatsura, J. F. Hartwig, *J. Am. Chem. Soc.* **2000**, *122*, 9546; b) O. Löber, M. Kawatsura, J. F. Hartwig, *J. Am. Chem. Soc.* **2001**, *123*, 4366; c) J. Pawlas, Y. Nakao, M. Kawatsura, J. F. Hartwig, *J. Am. Chem. Soc.* **2002**, *124*, 3669.

[11] T. Minami, H. Okamoto, S. Ikeda, R. Tanaka, F. Ozawa, M. Yoshifuji, *Angew. Chem.* **2001**, *113*, 4633; *Angew. Chem. Int. Ed.* **2001**, *40*, 4501.

[12] For computational mechanistic studies on transition metal assisted intermolecular hydroamination, see: a) B. F. Straub, R. G. Bergman, *Angew. Chem.* **2001**, *113*, 4768; *Angew. Chem. Int. Ed.* **2001**, *40*, 4632; b) H. M. Senn, P. E. Blöchl, A. Togni, *J. Am. Chem. Soc.* **2000**, *122*, 4098.

[13] There is substantial precedent for η^3-allylic structures in organo-f-element chemistry: a) G. Jeske, H. Lauke, H. Mauermann, P. N. Swepston, H. Schumann, T. J. Marks, *J. Am. Chem. Soc.* **1985**, *107*, 8091; b) E. Bunel, B. J. Burger, J. E. Bercaw, *J. Am. Chem. Soc.* **1988**, *110*, 976; c) S. P. Nolan, D. Stern, T. J. Marks, *J. Am. Chem. Soc.* **1989**, *111*, 7844; d) W. J. Evans, T. A. Ulibarri, J. W. Ziller, *J. Am. Chem. Soc.* **1990**, *112*, 2314; e) A. Scholz, A. Smola, J. Scholz, J. Löbel, H. Schumann, K.-H. Thiele, *Angew. Chem.* **1991**, *103*, 444; *Angew. Chem. Int. Ed. Engl.* **1991**, *30*, 435; f) W. J. Evans, R. A. Keyer, G. W. Rabe, D. K. Drummond, J. W. Ziller, *Organometallics* **1993**, *12*, 4664; g) W. J. Evans, S. L. Gonzales, J. W. Ziller, *J. Am. Chem. Soc.* **1994**, *116*, 2600.

[14] a) R. Taube, H. Windisch, F. Görlitz, H. Schumann, *J. Organomet. Chem.* **1993**, *445*, 85; b) R. Taube, H. Windisch, *J. Organomet. Chem.* **1994**, *472*, 71; c) R. Taube, St. Maiwald, J. Sieler, *J. Organomet. Chem.* **1996**, *513*, 37; d) R. Taube, H. Windisch, St. Maiwald, H. Hemling, H. Schumann, *J. Organomet. Chem.* **1996**, *513*, 49; e) R. Taube, H. Windisch, H. Weissenborn, H. Hemling, H. Schumann, *J. Organomet. Chem.* **1997**, *548*, 229; f) R. Taube, St. Maiwald, J. Sieler, *J. Organomet. Chem.* **2001**, *621*, 327.

[15] The following kinetics were experimentally determined for the intermolecular hydroamination of 1-trimethylsilylpropyne and *n*-propylamine mediated by $[Me_2SiCp'_2NdCH(TMS)_2]$: $\Delta H^{\neq} = 17.2$-(1.1) kcal mol^{-1} and $\Delta S^{\neq} = -25.9(9.7)$ cal mol^{-1} K^{-1}.[9b]

[16] a) R. Ahlrichs, M. Bär, M. Häser, H. Horn, C. Kölmel, *Chem. Phys. Lett.* **1989**, *162*, 165; b) O. Treutler, R. Ahlrichs, *J. Chem. Phys.* **1995**, *102*, 346; c) K. Eichkorn, O. Treutler, H. Öhm, M. Häser, R. Ahlrichs, *Chem. Phys. Lett.* **1995**, *242*, 652.

[17] a) P. A. M. Dirac, *Proc. Cambridge Philos. Soc.* **1930**, *26*, 376; b) J. C. Slater, *Phys. Rev.* **1951**, *81*, 385; c) S. H. Vosko, L. Wilk, M. Nussiar, *Can. J. Phys.* **1980**, *58*, 1200; d) A. D. Becke, *Phys. Rev.* **1988**, *A38*, 3098; e) J. P. Perdew, *Phys. Rev. B* **1986**, *33*, 8822; J. P. Perdew, *Phys. Rev. B* **1986**, *34*, 7406.

[18] See, for instance: a) S. Tobisch, Th. Nowak, H. Boegel, *J. Organomet. Chem.* **2001**, *619*, 24; b) H. Heiber, O. Gropen, J. K. Laerdahl, O. Swang, U. Wahlgreen, *Theor. Chem. Acc.* **2003**, *110*, 118.

[19] See, for instance: a) S. Tobisch, *Chem. Eur. J.* **2005**, *11*, 3113; b) S. Tobisch, *J. Am. Chem. Soc.* **2005**, *127*, in press.

[20] For further details, see www.struked.de.

[21] The thermodynamic gap between the prevalent s-*trans* and the s-*cis* configurations of 1,3-butadiene is 3.6/3.4 kcal mol^{-1} on the $\Delta H/\Delta G$ surface.

[22] Noteworthily, very similar energy profiles are also predicted for the *trans*-1,2 and *cis*-1,2 insertion pathways, which, however, does not have any mechanistic relevance, since these pathways remain almost entirely closed in the catalytic reaction course.

[23] J. Lukas, P. W. N. M. van Leeuwen, H. C. Volger, A. P. Kouwenhoven, *J. Organomet. Chem.* **1973**, *47*, 163.

[24] a) J. W. Faller, M. E. Thomsen, M. J. Mattina, *J. Am. Chem. Soc.* **1971**, *93*, 2642; b) K. Vrieze, *Fluxional Allyl Complexes in Dynamic Nuclear Magnetic Resonance Spectroscopy* (Eds.: L. M. Jackmann, F. A. Cotton), Academic Press, New York, **1975**.

[25] S. Tobisch, R. Taube, *Organometallics* **1999**, *18*, 3045.

[26] The free-energy barrier for allylic isomerization was determined by NMR spectroscopy to be about 16.0 kcal mol^{-1} for $[(\eta^5\text{-Cp}')La(\eta^3\text{-}C_3H_5)_3]^-$ (Cp′ = C_5H_5, C_5Me_5, C_9H_7, $C_{13}H_9$) complexes[14b] and greater than 15.5 kcal mol^{-1} for the $[La(\eta^3\text{-}C_3H_5)_3]$ dioxane adduct.[14d]

[27] Precursor isomers for protonation of the C^1 carbon atom bearing η^1(C^3)-butenyl–Nd and η^1-N-amine tether functionalities are disfavored by 1.9/2.1 kcal mol^{-1} (ΔG, *syn*/*anti*-butenyl form) relative to the favorable isomers shown in Figure 4.

[28] Examination by a linear-transit approach revealed no indication that amine association/dissociation is connected with a significant enthalpic barrier, which is in agreement with experimental findings.[7–9]

[29] Note that the condensed free-energy profile is computed for standard conditions (298.15 K, 1 atm, stoichiometric amounts of diene and amine substrates). The large excess of amine, however, favors the generation of adducts like **3**-AS. The correction of **3**+**1**→**3**-AS adduct formation for concentration effects according to $\Delta G = \Delta G° - RT\ln([\mathbf{3}\text{-AS}][\mathbf{3}]^{-1}[\mathbf{1}]^{-1}$, reduces the free energy by $RT\ln([\mathbf{1}]^{-1})$, which amounts to 2.0 kcal mol^{-1} when actual reaction conditions are considered (29-fold molar excess of **1**, 298.15 K, 1 atm[9c]).

[30] Total enthalpies (ΔH_{tot}) and free energies (ΔG_{tot}) and entropies (ΔS_{tot}) are given relative to the catalyst's resting state **3**-AS, corrected by the respective number of reactant molecules.

[31] J. H. Espenson, *Chemical Kinetics and Reaction Mechanism*, 2nd ed., McGraw-Hill, New York, **1995**.

[32] Rapid equilibrium conditions (i.e., $k_4[\mathrm{AS}] \gg k_{-3}$) were applied, which can reasonably be assumed for the kinetically highly mobile reactant association/dissociation.

[33] The rate law [Eq. (2)] also accounts for amine-inhibition effects that have been experimentally observed in intermolecular hydroamination of various C–C multiple bonds.[9a,b]

[34] Under similar assumptions as for Equation (2), one obtains: velocity = $K_1K_2k_3$[diene][**3**-AS][AS]$^{-1}$.

[35] See Schemes 3 and S1, respectively, by taking actual reaction conditions into account.[29]

[36] In the comparison of the energetics of alternative regioisomeric paths, the respective favorable stereochemical pathways were considered.

Received: March 29, 2005
Published online: August 5, 2005

